Parasite Epidemiology and Control 25 (2024) e00347

Contents lists available at ScienceDirect

Parasite Epidemiology and Control

journal homepage: www.elsevier.com/locate/parepi

Performance of ginger constituents against SARS-CoV-2 virus: A therapeutic and theoretical approach

Mustafa M. Kadhim [a], Anees A. Khadom [b,*], Jawad Kadhim Abaies [c], Wesam R. Kadhum [d], Safa K. Hachim [e]

[a] Department of Chemical and Petroleum Refinery, Kut University College, Kut, Wasit, Iraq
[b] Department of Chemical Engineering, College of Engineering, University of Diyala, Baquba City 32001, Daiyla Governorate, Iraq
[c] Department of Chemistry, College of Science, Wasit University, Wasit, Iraq
[d] Department of Pharmacy, Kut University College, Kut, Wasit 52001, Iraq
[e] National University of Science and Technology, Dhi Qar, Iraq

ARTICLE INFO

Keywords:
SARS-CoV-2
Ginger
DFT
Docking
Fukui

ABSTRACT

In the present research, ginger extracted compounds, namely; Gingerol {(1-[4′-hydroxy-3′-methoxyphenyl]-5-hydroxy-3-decanone} (1), Zingerone {(4-(4-Hydroxy-3-methoxyphenyl)-2-butanone)} (2), and Shogoals {(E)-1-(4-Hydroxy-3- methoxyphenyl) dec-4-en-3-one)} (3) have been investigated as SARS-Cov-2 inhibitors. The interaction of extracted compounds with the virus's spikes may restrict the virus's reproduction or give time to the body's immune system to detect viruses, consequently producing appropriate antibodies. Gaussian 09 with a 6-311G (d, p) basis set, UCA FUKUI, MGL implement, DSV, and LigPlus software were utilized. The active sites for adsorption were identified using the total electron density (TED), FUKUI function, and Millikan charges. Furthermore, docking analysis clearly showed that the inhibition of viral replication depends on binding energy (Eb) and ligand efficiency (LE). A docking study revealed that the inhibition ability of the studied compounds on SARS-CoV-2 was in the order of 2 > 3 > 1.

1. Introduction

Natural remedies for different kinds of sickness gained spreading popularity with continuously changing people's lifestyles. People around the world prefer natural products to synthetic ones because of their less harmful side effects. People are becoming more health-aware and nutritionally concerned, and they are increasingly turning to natural medicines for therapeutic reasons.

Ginger (*Zingiber officinale*), a well-known herbal plant, is a good option due to the high concentration of its physiologically active components. It is a powerful antioxidant with minimal disadvantages or unwanted reactions [1]. In addition, it aids in reactive species scavenging and the lowering of oxidative stressors in the body.

Ginger rhizomes are containing very important chemical constituents, which are volatile oils and non-volatile pungent compounds (Okamoto et al., 2011). Terpenoids are the main volatile compounds, while other volatile ones include paradol, zingerone, gingerol, and shagoal.

The fundamental features of ginger mainly belong to the zingerone, which is a major flavor component. Zingerone may assist in fighting against a variety of severe illnesses. It also increases respiratory burst, stimulates the immune system (Ownsend et al., 2013;

* Corresponding author.
E-mail address: aneesdr@gmail.com (A.A. Khadom).

https://doi.org/10.1016/j.parepi.2024.e00347
Received 11 August 2023; Received in revised form 31 March 2024; Accepted 5 April 2024
Available online 8 April 2024

Kumar et al., 2014a), phagocytic activity, resistance to infections, an excellent appetizer, consequently aiding in the development and maintenance of the body. Furthermore, it possesses anti-inflammatory effects (Zhang et al., 2016), can serve as a hepatoprotective agent (Kumar et al., 2014b), inhibits provoking intermediaries, and reduces inflammation and perniciousness, accordingly treating a wide range of inflammatory issues related to many diseases. Therefore, because of its many effects, zingerone has been thoroughly investigated, and surely there will be a future need for additional research on the medicinal properties of this natural molecule. Nonetheless, all of the zingerone's known metabolic activities may provide fresh insights into using this amazing natural chemical in therapy to avoid the adverse effects of synthetic medications.

Gingerols and shagoals are other important bioactive components of ginger. According to the previous studies, shagoals were produced by the dehydration of gingerols. It is also found that various temperatures and times affect the producing of shogaols from gingerols (Ghasemzadeh et al., 2018). It is worth mentioning that gingerols are found in higher concentrations than shogoals, but shogoals exhibited remarkable biological activities such as antitumor and antioxidant (Ghasemzadeh et al., 2015; Dugasani et al., 2010). It is also thought that both gingerol and shagoals are potentially valuable in influencing weight reduction because they induce transient receptor potential vanilloid-1 (TRPV1) (Okamoto et al., 2011; Iwasaki et al., 2006). In this context, they may be analogous to capsaicin, a compound found in chili peppers with different pharmacological and physiological effects such as anti-cancer, anti-oxidant, and anti-obesity.

For more than two years, the world is facing a major health threat, namely COVID-19. The Epidemic was generated by the SARS-CoV-2 virus, recognized for the first time in Wuhan, China (Ji et al., 2017). The number of positive cases continues to grow every day, and it is predicted to grow over time. With this crisis, there is urgent to develop an agent to prevent or at least reduce the COVID-19

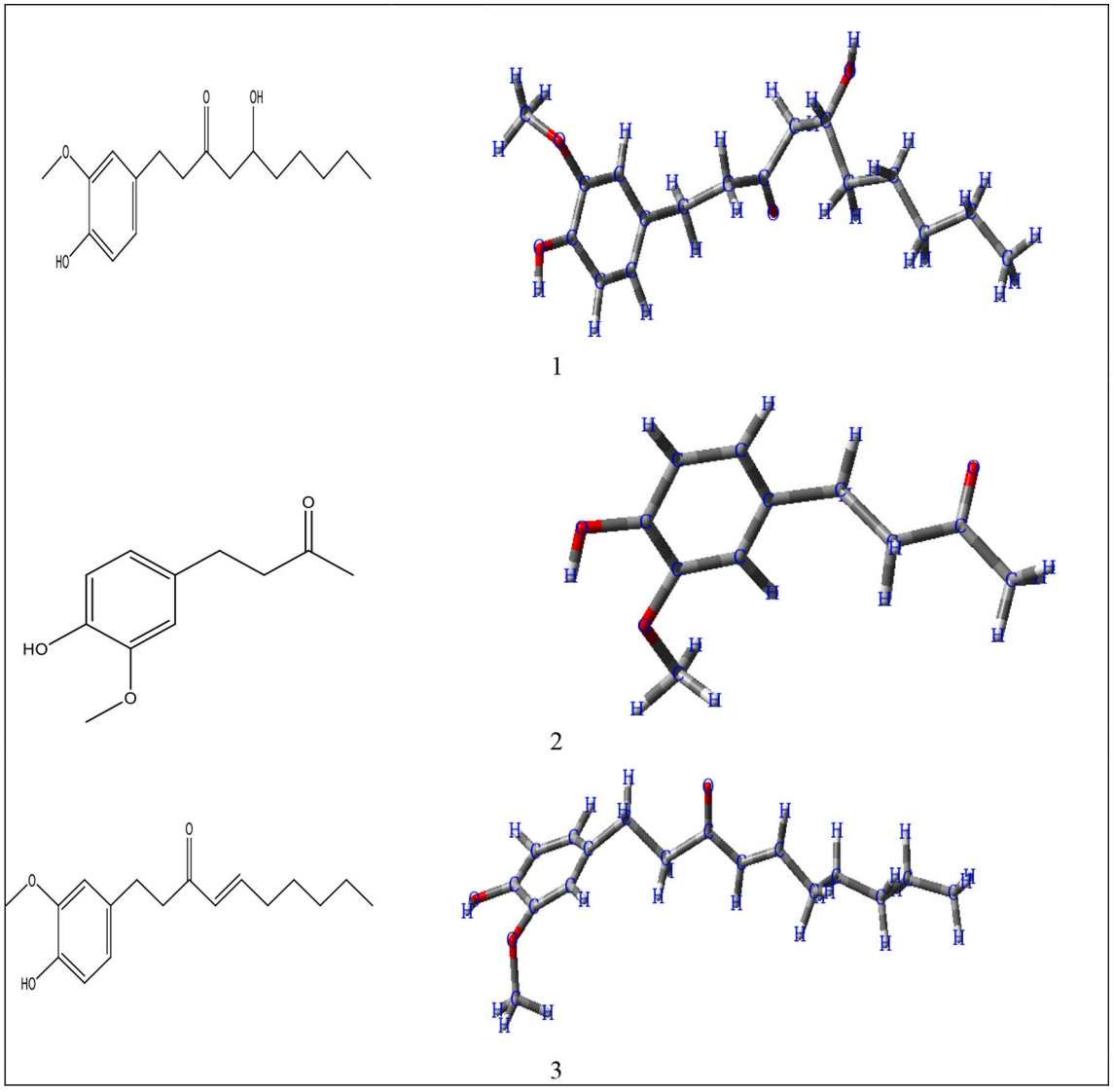

Fig. 1. 2D and 3D structures of the studied compounds.

outbreak. Spike (S) is one of the SARS-CoV2 proteins involved in viral entry during infection. They target the host cell's Angiotensin-Converting Enzyme 2 (ACE2) receptor, creating a conducive environment for viral replication. Due to its importance, many drug developments have targeted S protein to prevent disease (Abolaji et al., 2017; Zhang et al., 2013).

Natural-derived compounds are gaining recognition as a potential therapeutic option for various diseases, including viral infection. Herbal research is underway intending to decrease sickness caused by coronavirus (Moon et al., 2018; Suk et al., 2017).

The current study aimed to explore the antiviral properties of Ginger and the possibility of counteracting SARS-CoV-2 infection based on ligand interaction with the spike proteins. In silico test for active compounds in the Ginger was carried out using docking calculations on S protein, which revealed a good activity of the tested compounds. Therefore, depending on the carried out study, we think that several active compounds in Ginger could block the ACE2 receptor from binding to the S protein.

2. Material and methods

2.1. Quantum chemical calculations

In the current study, quantum chemical calculations were performed using density functional theory (DFT) with the Becke three-parameter hybrid function, specifically the Lee, Yang, and Parr (B3LYP) functional, implemented through Gaussian 09 software. The chosen 6-311G (d, p) basis set, known for its accuracy in describing electronic properties and molecular conformations, was employed. The computational approach focuses on the efficient modeling of electronic structure, utilizing a widely accepted hybrid functional and a basis set designed to capture both electronic correlation effects and polarization. The study aims to provide precise insights into the molecular properties of the investigated compounds, as represented visually in Fig. 1, combining the computational efficiency of DFT with the accuracy afforded by the selected methods and basis set (Khudhair et al., 2021).

2.2. Protein data

In the current research, the Research Collaboratory for Structural Bioinformatics (RCSB) (Li et al., 2012) played a pivotal role as a comprehensive repository, facilitating the retrieval of intricate protein conformations. Complementarily, the Molecular Graphic Laboratory (MGL) tools were instrumental in conducting Autodock calculations with a nuanced approach (Kadhim et al., 2021; Brendler et al., 2021). The Autodock technique (ADT, version 1.5.6) was strategically employed to delve into the intricate coordination dynamics between the SARS-CoV-2 spike glycoprotein-S1 and the ligands (1, 2, and 3). Ensuring the meticulous preparation of inputs for ADT analysis, the spike glycoprotein-S1 and ligand conformations underwent a transformation to a format compatible with ADT (*. pdbqt files). This preparatory step involved the addition of exhaustive hydrogen atoms and Gasteiger charges, ensuring a more accurate representation (Sayin et al., 2019). It's noteworthy that the Autodock algorithm autonomously determined the molecular root, an aspect subject to user specifications if required. Expanding the analytical spectrum, AutoGrid (version 4.2.6) was strategically harnessed to compute comprehensive atom-specific affinity maps, encompassing electrostatic and desolation potentials for all ligand atoms. Prior to the actual docking calculations, the ligands underwent meticulous optimization in the gas phase. Furthermore, the study extended its scope by delving into the molecular electrostatic potential (TED) and Fukui function, leveraging the inherent capabilities of the available Density Functional Theory (DFT) method (Zimmermann-klemd et al., 2020; Yu et al., 2018). This exhaustive and intricate methodology was meticulously crafted, underscoring a commitment to precision and depth in unraveling the complex interactions between the ligands and the SARS-CoV-2 spike glycoprotein-S1.

3. Results and discussion

3.1. Effect of molecular orbital on activity

In this section, a number of physical properties related to the activity of studied compounds (B. AD, 1993; Lee et al., 1988) are investigated. Regarding E_{LUMO}, the order was $3 < 1 < 2$, as the low value of this factor, means a high activity. The energy gap, which is the difference between energy level of HOMO and energy level of LUMO, the order was $3 < 2 < 1$. Electronegativity (χ) refers to the attraction tendency of shared electrons by atom. The decrease in (χ) resulting in increase of the activity. The second derivative of E is called the Hardness (η), which indicates the molecule reactivity or molecule stability. The inverse of the global hardness (η) is the global softness (σ), which is an essential property for deciding molecular reactivity and stability. The high value of the dipole moment (μ) is corresponding to the high activity. Table 1 represents the studied parameters of the studied compounds. As a result, the following will be the order of activity according to the parameters in Table 1; **1 < 2 < 3**. In addition, eqs. 1 through 5 are used in parameters

Table 1
Calculated E_{HOMO}, E_{LUMO}, energy bandgap ($\Delta E = E_{HOMO} - E_{LUMO}$), chemical potential ($\mu$), electronegativity ($\chi$), global hardness ($\eta$), global electrophilicity index (ω), and softness (σ) for compounds **1–3**.

Comp.	E_{HOMO} / eV	E_{LUMO} / eV	ΔE /eV	χ / eV	μ / eV	η / eV	σ / eV-1	ω / eV	Electronic Energy	Dipole Moment
1	−6.1047	−0.7714	5.3332	3.4381	−3.4381	2.6666	0.3750	2.2163	−964.330	2.1562
2	−5.8089	−0.5967	5.2121	3.2028	−3.2028	2.6060	0.3837	1.9681	−653.379	4.4756
3	−5.9118	−1.9619	3.9498	3.9368	−3.9369	1.9749	0.5063	3.9240	−888.057	4.4877

calculations.

$$IE = -E_{HOMO} \tag{1}$$

$$EA = -E_{LUMO} \tag{2}$$

$$\eta = \frac{IE - EA}{2} \tag{3}$$

$$\sigma = \frac{1}{\eta} \tag{4}$$

$$X = \frac{IE + EA}{2} \tag{5}$$

3.2. The active sites on the molecules

Fig. 2 presents the meticulously optimized geometries of the investigated molecules, scrutinized within the confines of the gas phase. The depiction encompasses a thorough analysis of the density distribution of the Highest Occupied Molecular Orbital (HOMO) and Lowest Unoccupied Molecular Orbital (LUMO). In this representation, red regions signify heightened electron density, indicative of regions where electrons are abundant, while green regions denote areas of lower electron density (Yaqo et al., 2019). Notably, the areas characterized by high electron density (red regions) serve as zones where electrons are primed for donation to the receptor, thereby influencing bond formation and adsorption dynamics. The electron density at the donor atom plays a critical role in shaping these interactions. Figure 2: further introduces the concept of Total Electron Density (TED) as a key metric for illustrating the overall electronic density across the molecule.

Expanding our analytical lens to Fig. 3, the color-coded representation offers nuanced insights into the electronic characteristics of the studied molecules. The red areas signify atoms with elevated electron negativity, prominently observed in elements like oxygen, thereby implying their potential role in nucleophilic attacks. Atoms characterized by moderate electronegativity are designated with a yellow color, presenting a balanced electron affinity. Conversely, the blue-colored regions highlight atoms exhibiting the highest electro positivity, showcasing their predisposition to accept electrons from donors (Kadhim and Kubba, 2020a). This detailed comparison enhances our understanding of the electronic properties, reactivity, and potential chemical interactions within the studied molecular systems.

3.3. Electrophilic and nucleophilic attack

The Fukui function (fx), derived from the derivative of electron density concerning the number of electrons (N) at a constant external potential, emerges as a pivotal tool for discerning active sites within functional groups of optimal conformations (Radhi et al., 2020; Kadhim and Kubba, 2020b). In this comprehensive study, the Fukui and Dual Descriptor (D·D) values were meticulously computed through the utilization of the Density Functional Theory (DFT) technique, employing the 6-311G/d, p basis set, Gaussian 09

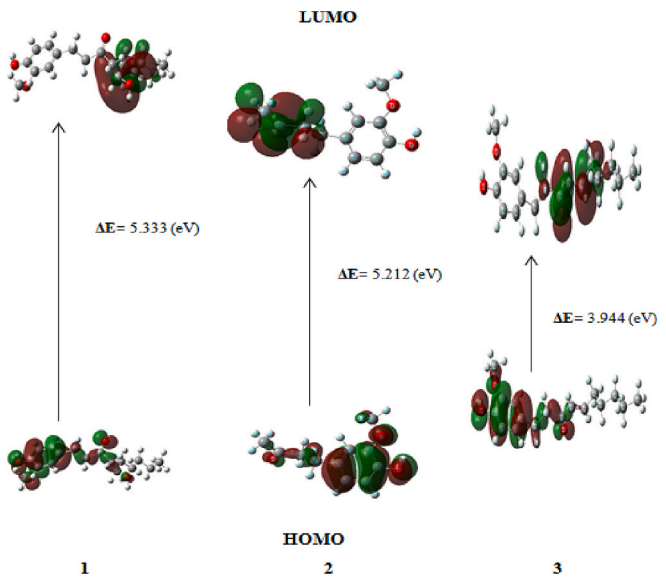

Fig. 2. The molecular orbitals (HOMO-LUMO) of the compounds **1**, **2,** and **3**.

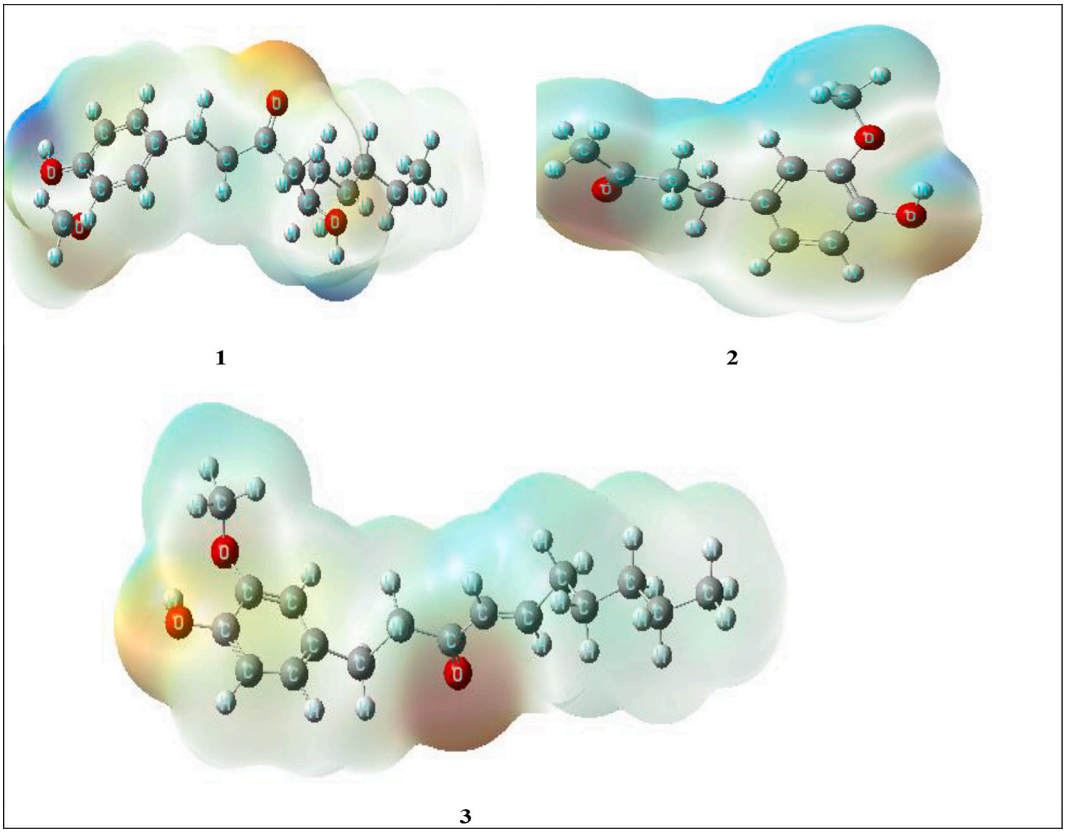

Fig. 3. Electron distribution according to TED map.

software, and the USA FUKUI software. The nuanced calculation revealed that the (f+) parameter characterizes the electron-accepting ability, while (f-) signifies the electron-donating capability. The Dual Descriptor plays a crucial role in distinguishing between electrophilic (+) and nucleophilic (−) atoms (see Fig. 4).

Delving into the nucleophilic and electrophilic behavior of individual atoms within compounds 1, 2, and 3, a comprehensive list of nucleophilic atoms was identified, including C1, C2, C3, C4, O11, O12, C13–18, O19, C20, O21, H22, H23, H27, H41, and H43 in compound 1, denoting their propensity for electron donation. Conversely, other atoms were classified as electrophilic, showcasing a clear distinction in their electron-accepting behavior (Table 2).

The Fukui function went a step further in pinpointing the most electrophilic and nucleophilic atoms within each compound. Notably, C7, C6, H28, and H32 were highlighted as the most electrophilic in compound 1, while C10, C12, O14, H24, and H28 took the lead in compound 2, and C3, C4, and H22 were identified in compound 3. Concurrently, nucleophilic atoms were revealed, such as C13, C15, C16, and O21 in compound 1, C2, C3, C5, O7, O8, and H22 in compound 2, and C2, C12, C13, C14, and H44 in compound 3, signifying their avidity for electron donation. The DFT technique was employed to delve into the reactive centers, scrutinizing nucleophilic and electrophilic tendencies. The study elucidated that the electron density serves as a vital parameter for estimating chemical reactivity. Regions with larger electronic charge were identified as softer, exhibiting a greater predisposition to electrostatic interactions. Charges on molecules were highlighted for their profound influence on physicochemical characteristics, ultimately determining electrophilic attack centers.

A closer examination of compounds 1, 2, and 3 unveiled electrophilic attack centers, emphasizing the most active centers capable of accepting electrons, specifically involving C, H atoms, and the carbon of carbonyl groups (Fig. 5). This insightful analysis underscored that the most reactive compounds (1, 2, and 3) exhibit O, C, and H atoms carrying a negative charge. The Millikan charge, a crucial authorization for Fukui function predictions, further validated the reactivity patterns observed.

In essence, this intricate and exhaustive analysis not only elucidates the specific active centers within the studied molecules but also contributes to a nuanced interpretation of their reactivity patterns. The Fukui function, Dual Descriptor, and DFT techniques collectively provide a robust framework for understanding molecular behavior and reactivity at a fundamental level (Frisch et al., 2009; Li et al., 2014a). The elucidation of nucleophilic and electrophilic tendencies, coupled with the identification of specific active centers, enriches our understanding of the intricate interplay of electrons within these compounds, paving the way for informed predictions and applications in diverse fields.

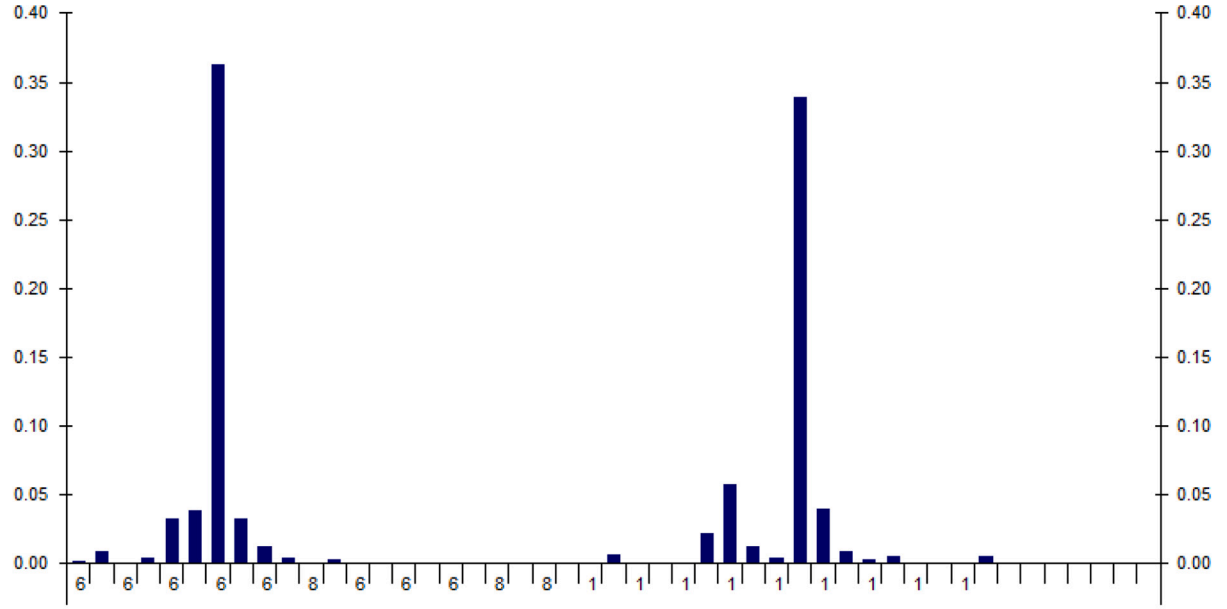

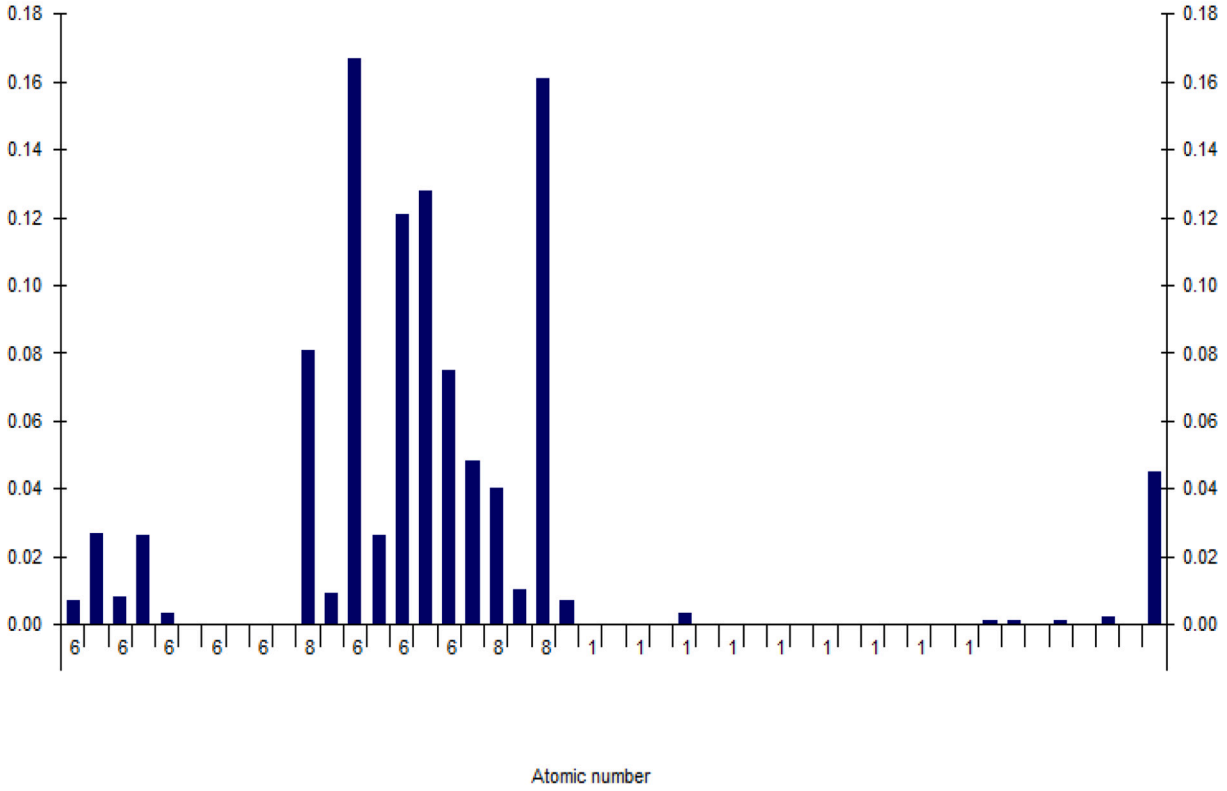

A

Fig. 4. Fukui charts of compound (A) 1, (B) 2, and (C) 3.

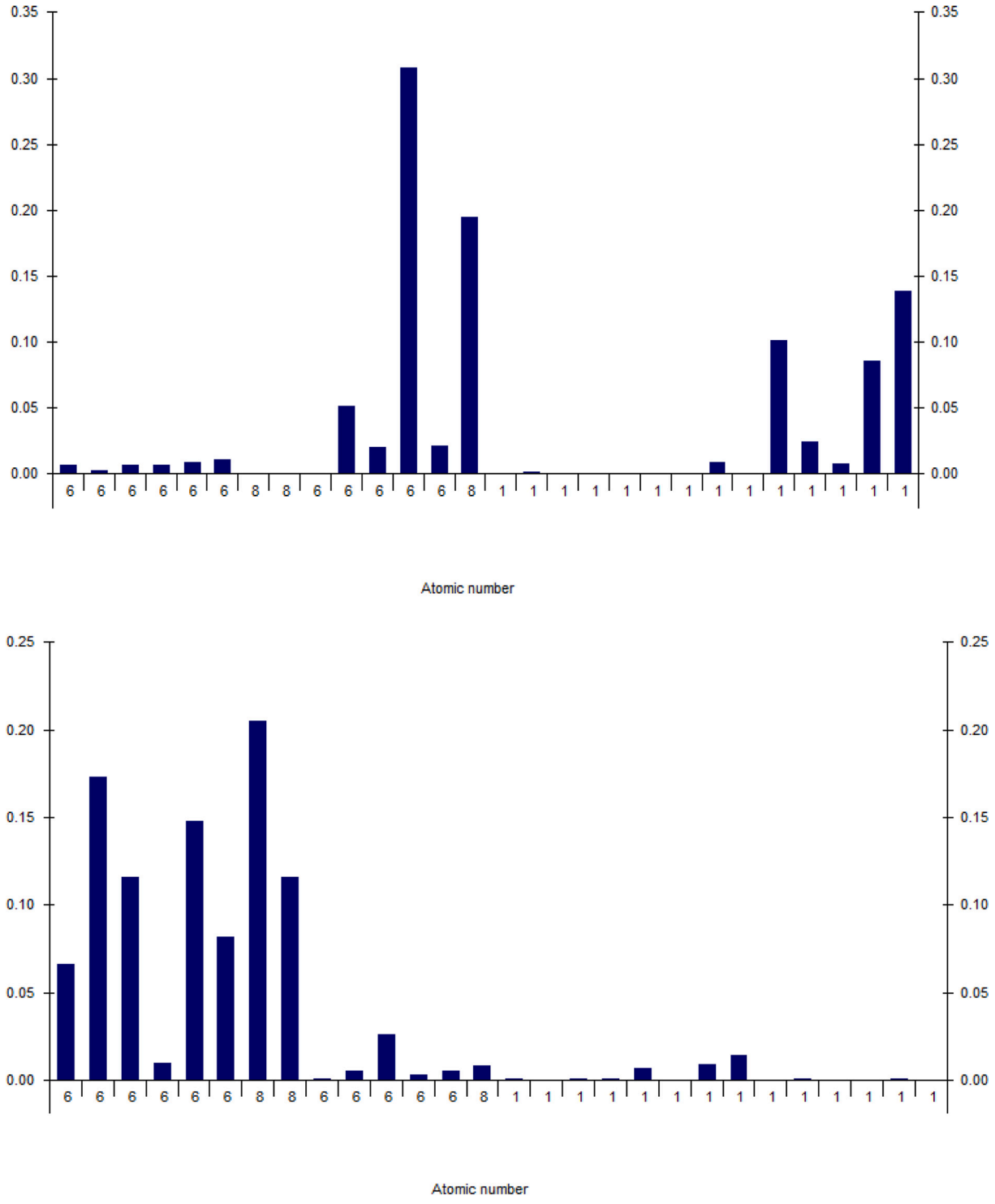

B

Fig. 4. (*continued*).

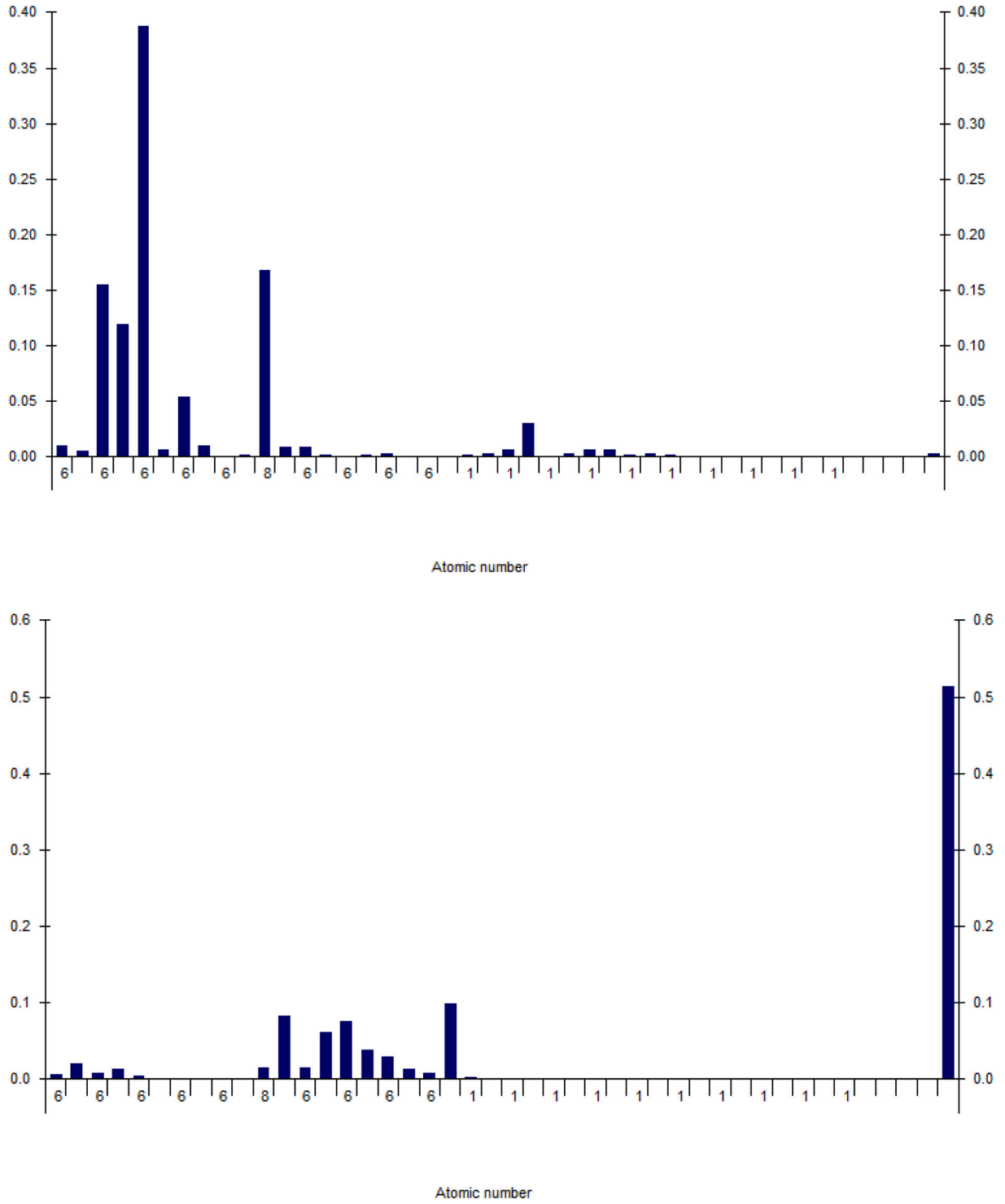

C

Fig. 4. (*continued*).

Table 2
FUKUI function and dual descriptor of the studied compounds.

1				2				3			
No	f^+	f^-	D·D	No	f^+	f^-	D·D	No	f^+	f^-	D·D
C1	6×10^{-4}	6.8×10^{-3}	-6.2×10^{-3}	C1	5.8×10^{-3}	6.5×10^{-2}	−0.0600	C1	9.6×10^{-3}	6.2×10^{-3}	3.4×10^{-3}
C2	9×10^{-3}	2.7×10^{-2}	-1.8×10^{-2}	C2	1.6×10^{-3}	0.1728	−0.1712	C2	5.2×10^{-3}	0.0192	-1.4×10^{-2}
C3	4×10^{-4}	7.9×10^{-3}	-7.5×10^{-3}	C3	5.8×10^{-3}	0.1161	−0.1103	C3	0.1536	7.6×10^{-3}	0.1460
C4	3.7×10^{-3}	2.6×10^{-2}	-2.3×10^{-2}	C4	6.5×10^{-3}	1×10^{-2}	-4×10^{-3}	C4	0.1191	0.0119	0.1072
C5	3.2×10^{-2}	2.9×10^{-3}	2.9×10^{-2}	C5	8.4×10^{-3}	0.1485	−0.1401	C5	0.3876	2.5×10^{-3}	0.3851
C6	3.8×10^{-2}	1×10^{-4}	3.8×10^{-2}	C6	1.1×10^{-2}	8.2×10^{-2}	−0.0706	C6	6.3×10^{-3}	3×10^{-4}	6×10^{-3}
C7	0.3631	3×10^{-4}	0.3628	O7	1×10^{-4}	0.2051	−0.2051	C7	5.3×10^{-2}	0	5.3×10^{-2}
C8	3.2×10^{-2}	1×10^{-4}	3.2×10^{-2}	O8	4×10^{-4}	0.1165	−0.1161	C8	1×10^{-2}	0	1×10^{-2}
C9	1.2×10^{-2}	0	1.1×10^{-2}	C9	4×10^{-4}	6×10^{-4}	-3×10^{-4}	C9	4×10^{-4}	0	4×10^{-4}
C10	3.6×10^{-3}	0	3.6×10^{-3}	C10	5×10^{-2}	4.8×10^{-3}	0.0460	C10	1×10^{-3}	0	1×10^{-3}
O11	2×10^{-4}	8.1×10^{-2}	-8.1×10^{-2}	C11	1.9×10^{-2}	0.0258	-6.2×10^{-3}	O11	0.1683	1.5×10^{-2}	0.1531
O12	2.6×10^{-3}	9.5×10^{-3}	-6.9×10^{-3}	C12	0.3078	3.5×10^{-3}	0.3043	C12	8.3×10^{-3}	8.3×10^{-2}	-7.4×10^{-2}
C13	4×10^{-4}	0.1666	−0.1662	C13	2.1×10^{-2}	5.3×10^{-3}	0.0158	C13	9×10^{-3}	1.5×10^{-2}	-5.9×10^{-3}
C14	2×10^{-4}	2.6×10^{-2}	-2.6×10^{-2}	O14	0.1947	8.1×10^{-3}	0.1866	C14	1.4×10^{-3}	6×10^{-2}	-5.9×10^{-2}
C15	0	0.1213	−0.1213	H15	3×10^{-4}	7×10^{-4}	-4×10^{-4}	C15	4×10^{-4}	7.4×10^{-2}	-4.7×10^{-2}
C16	1×10^{-4}	0.1279	−0.1278	H16	6×10^{-4}	0	6×10^{-4}	C16	9×10^{-4}	3.8×10^{-2}	-3.7×10^{-2}
C17	0	7.5×10^{-2}	-7.5×10^{-2}	H17	1×10^{-4}	8×10^{-4}	-6×10^{-4}	C17	1.7×10^{-3}	2.9×10^{-2}	-2.7×10^{-2}
C18	2×10^{-4}	4.8×10^{-2}	-4.7×10^{-2}	H18	0	1.2×10^{-3}	-1.2×10^{-3}	O18	1×10^{-4}	1.3×10^{-2}	-1.3×10^{-2}
O19	0	4×10^{-2}	-4×10^{-2}	H19	3×10^{-4}	7.5×10^{-3}	-7.1×10^{-3}	C19	0	6.9×10^{-3}	-6.8×10^{-3}
C20	0	1×10^{-2}	-1×10^{-2}	H20	0	0	0	O20	1×10^{-4}	9.9×10^{-2}	-9.9×10^{-2}
O21	0	0.16	−0.1610	H21	0	8.5×10^{-3}	-8.5×10^{-3}	H21	1.4×10^{-3}	2.4×10^{-3}	-1×10^{-3}
H22	1×10^{-4}	7.1×10^{-3}	-7×10^{-3}	H22	7.8×10^{-3}	1.4×10^{-2}	-6.4×10^{-3}	H22	3.3×10^{-3}	0.0015	1.8×10^{-3}
H23	0	4×10^{-4}	-4×10^{-4}	H23	5×10^{-4}	4×10^{-4}	1×10^{-4}	H23	6.4×10^{-3}	1×10^{-4}	6.4×10^{-3}
H24	6×10^{-3}	3×10^{-4}	5.6×10^{-3}	H24	0.1013	1×10^{-3}	0.1003	H24	3×10^{-2}	0	3×10^{-2}
H25	2×10^{-4}	1×10^{-4}	2×10^{-4}	H25	2.5×10^{-2}	0	2.4×10^{-2}	H25	3×10^{-4}	1×10^{-4}	2×10^{-4}
H26	1×10^{-4}	1×10^{-4}	0	H26	7.4×10^{-3}	1×10^{-4}	7.3×10^{-3}	H26	2.5×10^{-3}	1×10^{-4}	2.4×10^{-3}
H27	2×10^{-4}	3.2×10^{-3}	-3×10^{-3}	H27	8.5×10^{-2}	5×10^{-4}	8.4×10^{-2}	H27	6.3×10^{-3}	0	6.2×10^{-3}
H28	2.2×10^{-2}	5×10^{-4}	2.1×10^{-2}	H28	0.1380	1×10^{-4}	0.1379	H28	5.9×10^{-3}	0	5.9×10^{-3}
H29	5.8×10^{-2}	0	5.7×10^{-2}	–	–	–	–	H29	7×10^{-4}	0	7×10^{-4}
H30	1.2×10^{-2}	0	1.2×10^{-2}	–	–	–	–	H30	1.6×10^{-3}	0	1.6×10^{-3}
H31	4.1×10^{-3}	1×10^{-4}	4×10^{-3}	–	–	–	–	H31	8×10^{-4}	0	8×10^{-4}
H32	0.3391	0	0.3390	–	–	–	–	H32	2×10^{-4}	0	2×10^{-4}
H33	3.9×10^{-2}	0	3.9×10^{-2}	–	–	–	–	H33	0	0	0
H34	9.4×10^{-3}	0	9.4×10^{-3}	–	–	–	–	H34	5×10^{-4}	0	5×10^{-4}
H35	3.2×10^{-3}	0	3.2×10^{-3}	–	–	–	–	H35	3×10^{-4}	0	3×10^{-4}
H36	4.5×10^{-3}	0	4.5×10^{-3}	–	–	–	–	H36	0	0	0
H37	0	0	0	–	–	–	–	H37	0	0	0
H38	1×10^{-4}	0	1×10^{-4}	–	–	–	–	H38	2×10^{-4}	8×10^{-4}	-5×10^{-4}
H39	1×10^{-4}	0	1×10^{-4}	–	–	–	–	H39	0	3×10^{-4}	-3×10^{-4}
H40	5.2×10^{-3}	7×10^{-4}	4.5×10^{-3}	–	–	–	–	H40	0	1×10^{-4}	0
H41	0	1.4×10^{-3}	-1.4×10^{-3}	–	–	–	–	H41	0	0	0
H42	0	1×10^{-4}	-1×10^{-4}	–	–	–	–	H42	0	3×10^{-4}	-3×10^{-4}
H43	0	7×10^{-4}	-6×10^{-4}	–	–	–	–	H43	0	4×10^{-4}	-4×10^{-4}
H44	0	3×10^{-4}	-3×10^{-4}	–	–	–	–	H44	3.2×10^{-3}	0.5129	−0.5096
H45	0	1.7×10^{-3}	-1.7×10^{-3}	–	–	–	–	–	–	–	–
H46	0	1×10^{-4}	-1×10^{-4}	–	–	–	–	–	–	–	–
H47	1×10^{-4}	4.5×10^{-2}	-4.5×10^{-2}	–	–	–	–	–	–	–	–

3.4. Interaction of inhibitors with the virus spikes

The potential mechanisms underlying the suppression of the SARS-CoV-2 virus by compounds 1, 2, and 3 involve their interaction with viral spikes, presenting an avenue for enhancing immune system engagement. Geometry optimization reveals that the reactive functional groups crucial for inhibitory actions are the hydroxyl (OH) and carbonyl (C=O) groups. Notably, certain regions exhibit planarity, aligning with the cis and trans conformations of molecule atoms. The dihedral angle analysis underscores this, with the near-zero dihedral angle for cis conformations and approximately 180 degrees for trans conformations. The structural code (6acd) of the viral spikes, obtained from the Protein Data Bank (PDB), is illustrated in Fig. 6. The interaction of the active compounds 1, 2, and 3 with the viral protein was assessed to identify the most favorable binding sites. This evaluation was based on measuring the binding energy or affinity of the inhibitors with the receptor, providing crucial insights into their potential efficacy (Yousef and Al-nassiry, 2020; Abdul et al., 2021). The root mean square deviation (RMSD) values for the studied compounds were determined as 63.98, 27.06, and 9.51 for 1, 2, and 3, respectively. These values reflect the deviation from the optimal structure and offer insights into the stability of the interactions.

The range of binding energy (kcal/mol) for compounds 1, 2, and 3 was observed as −0.60 to −2.66, −2.83 to −3.83, and − 1.92 to −3.45, respectively (Table 3). The comparison of binding energy values reveals that compound 2 exhibits the strongest interaction with the viral spikes, followed by compounds 3 and 1. This hierarchy suggests varying degrees of effectiveness in inhibiting viral

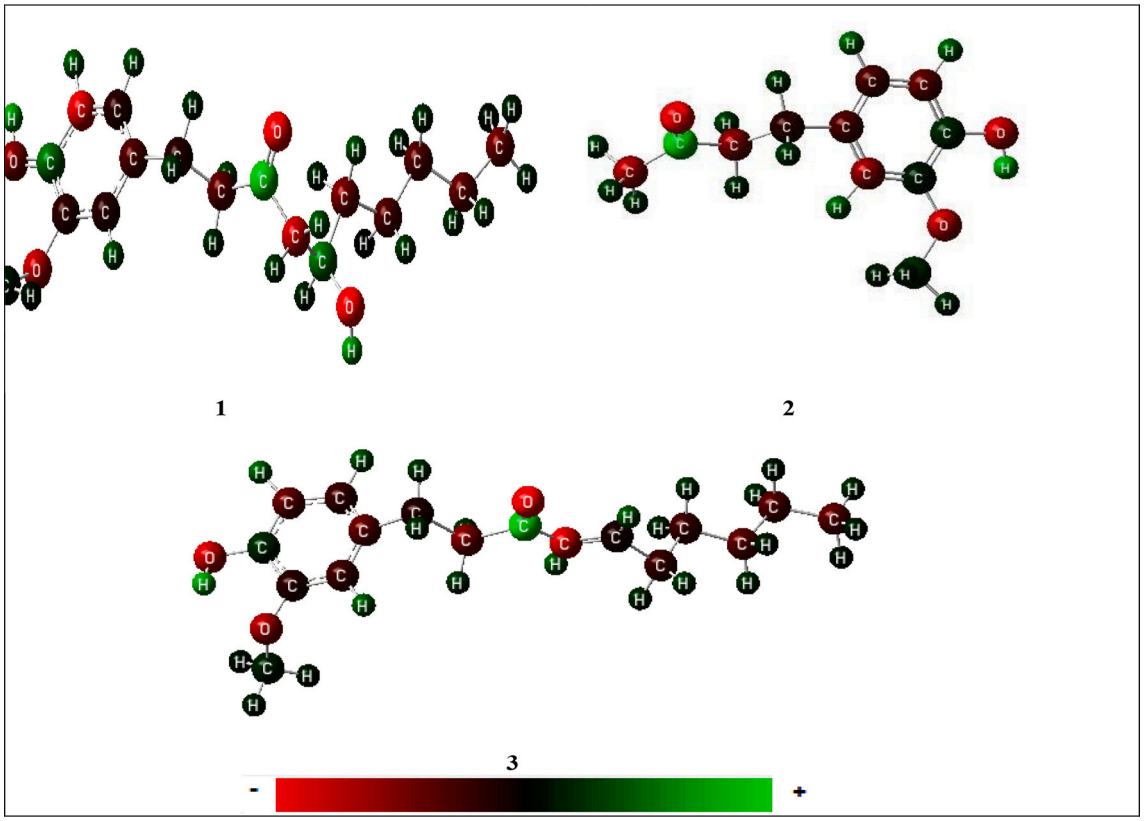

Fig. 5. Distribution of Millikan charges on compounds structures.

activity. Additionally, the Ligand Efficiency (LE) per atom in the ligand to the receptor protein was calculated as −0.13, −0.27, and −0.17 kcal/mol for inhibitors 1, 2, and 3, respectively (Eva et al., 2019; Li et al., 2014b). These LE values provide insights into the efficiency of each compound in terms of interactions with the receptor protein on a per-atom basis. The cumulative findings suggest that these proposed inhibitors may afford the body sufficient time to develop specific antibodies capable of resisting the targeted virus. The detailed examination of binding energies, RMSD values, and Ligand Efficiency provides a comprehensive understanding of the interactions between the compounds and viral spikes, laying the groundwork for potential therapeutic interventions.

Fig. 7 delineates the active sites crucial for the acceptance and donation of hydrogen bonds within the receptor. These sites play a pivotal role in molecular interactions, facilitating the formation of hydrogen bonds that are instrumental in the binding process. The depiction of these active sites provides a visual guide to the specific regions where hydrogen bond interactions occur, shedding light on the intricate molecular recognition patterns. Moreover, the hydrophilic and hydrophobic properties of materials play a significant role in dictating their affinity towards water molecules. Fig. 8 serves as a comprehensive representation of these properties, illustrating the intricate balance between hydrophilicity and hydrophobicity. The blue-colored regions signify more negative areas, characterizing hydrophilic regions with a propensity to interact favorably with water molecules. Conversely, the red-colored regions denote more positive areas, indicative of hydrophobic regions that tend to repel water molecules. This detailed analysis of the hydrophilic and hydrophobic properties offers valuable insights into the materials' molecular characteristics, contributing to a nuanced understanding of their interactions with the surrounding environment. Such insights are crucial in the design and optimization of materials for specific applications, particularly in contexts where interactions with water molecules play a significant role.

3.5. Bonds of inhibitors with the virus's amino acids

The intricate interplay between the amino acids constituting the viral spikes and the proposed inhibitors (compounds 1, 2, and 3) is meticulously examined through a comprehensive analysis employing DSV, LigPlus, and MGL tools, as elucidated in Fig. 9. Compound 1 manifests a diverse array of interactions, notably hydrogen bonding with Leucine (LEU) and Lysine (LYE), along with alkyl and pi-alkyl interactions involving Cysteine (CYS) and Alanine (ALA). In a parallel fashion, Compound 2 showcases a similarly intricate interaction profile. This includes hydrogen bonding with oxygen atoms, OH, and C═O groups in Serine (SER), Glycine (GLY), and Asparagine (ASN), alkyl interaction with Glutamine (GLU), and pi-alkyl interaction with Isoleucine (ILE). Additionally, a notable C—H interaction is observed with Tyrosine (TYR). Compound 3, similarly, demonstrates a multi-faceted interaction repertoire with the viral spikes. This includes hydrogen bonding with Serine (SER), Valine (VAL), and Arginine (ARG), as well as alkyl and pi-alkyl interactions involving

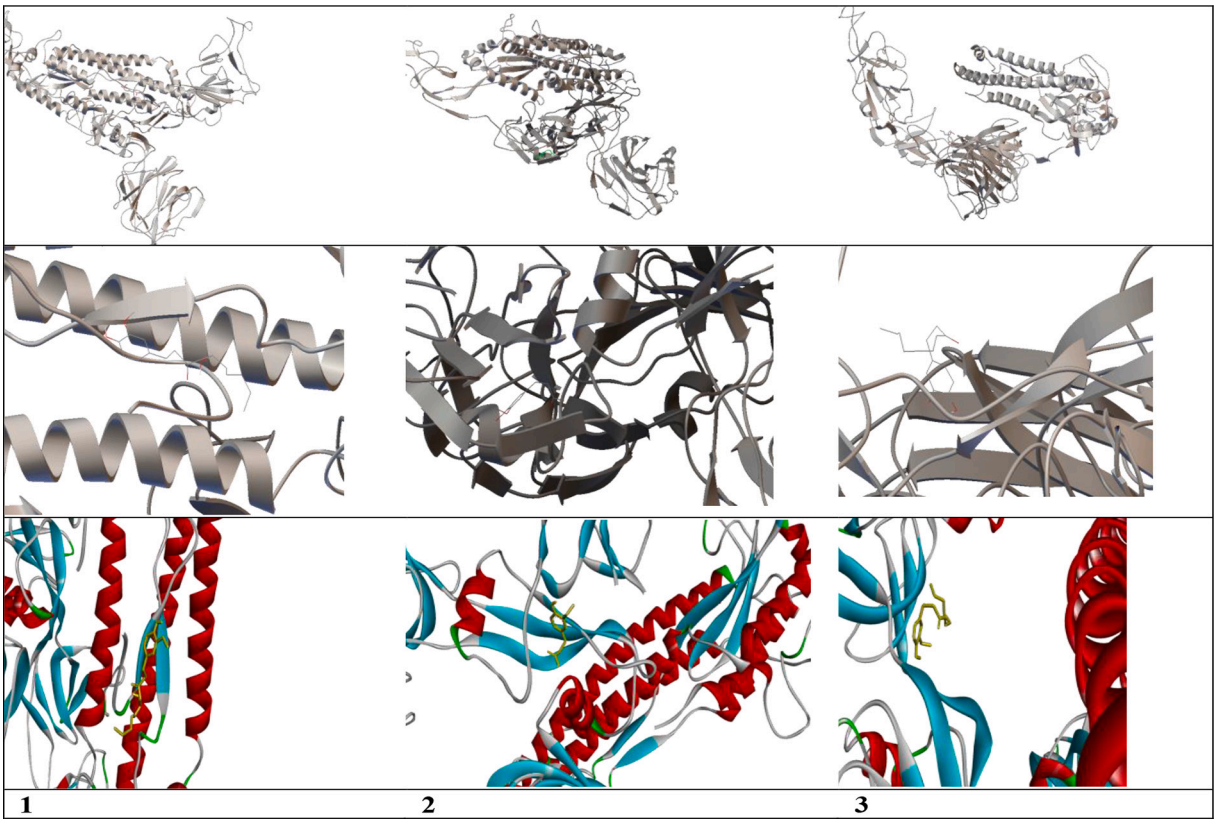

Fig. 6. Protein structure with compounds 1, 2, and 3.

Table 3
Values of binding energy and ligand efficiency of the studied compounds.

Comp.	Eb (kcal/mol)	LE	Eb range	Best site number	RMSD
1	−2.66	−0.13	−0.60 to −2.66	3	63.98
2	−3.83	−0.27	−2.83 to −3.83	10	27.06
3	−3.45	−0.17	−1.92 to −3.45	9	9.51

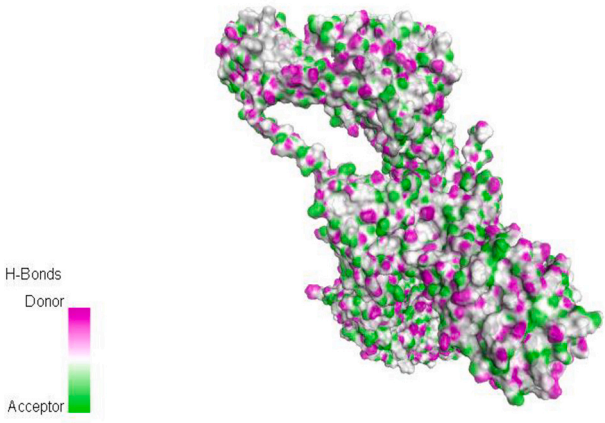

Fig. 7. H-bond donor and acceptor sites on the spikes structure.

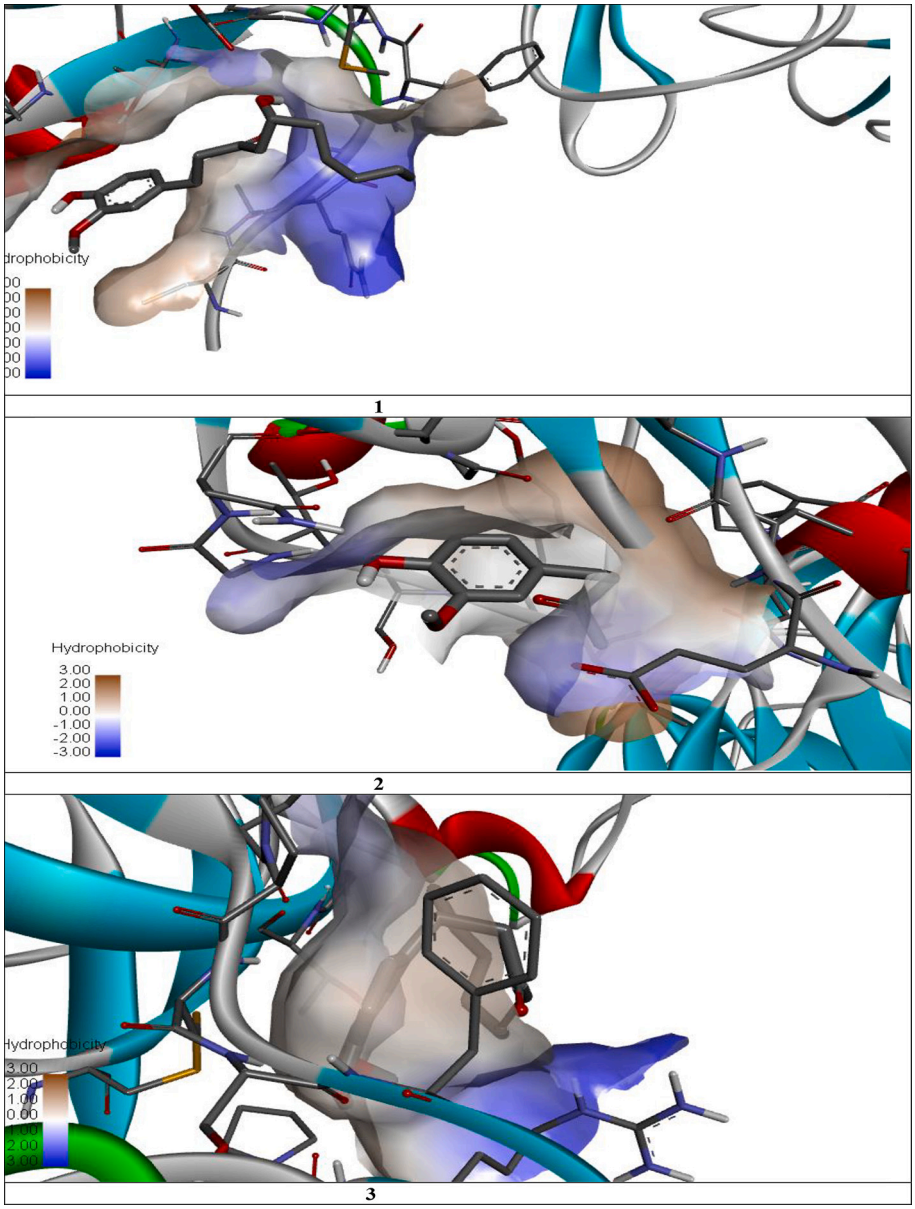

Fig. 8. Hydrophilic and hydrophobic sites in the linkage area of inhibitors and spikes.

Proline (PRO) and Cysteine (CYS), with the latter interacting with the pi electrons of the aromatic ring.

Further insight into the strength of these interactions is gained by examining the bond lengths of specific hydrogen bonds. For instance, the hydrogen bond lengths for LYS-Ccompound 1, GLY-Ccompound 2, SER-Ccompound 2, ARG-Ocompound 3, and VAL-Ocompound 3 are measured at 3.01, 3.02, 3.17, 3.12, and 2.86 Å, respectively (Fig. 6). The short bond lengths observed in these interactions signify strong linkages, thereby indicating the robust efficiency of compounds 2 and 3. This analysis not only dissects the specific types of interactions but also provides a quantitative measure of their strength, establishing a hierarchy of efficacy among the proposed inhibitors.

In summary, the detailed examination of the interaction profiles between the proposed inhibitors and viral spikes unveils a nuanced understanding of the molecular dynamics at play. This insight is crucial for delineating the specific mechanisms through which compounds 1, 2, and 3 exert their inhibitory effects, paving the way for informed drug design and therapeutic interventions. The hierarchy of interaction strengths provides valuable information for further optimization and refinement of these compounds for enhanced antiviral efficacy (Hussein et al., 2020; Mustafa et al., 2021).

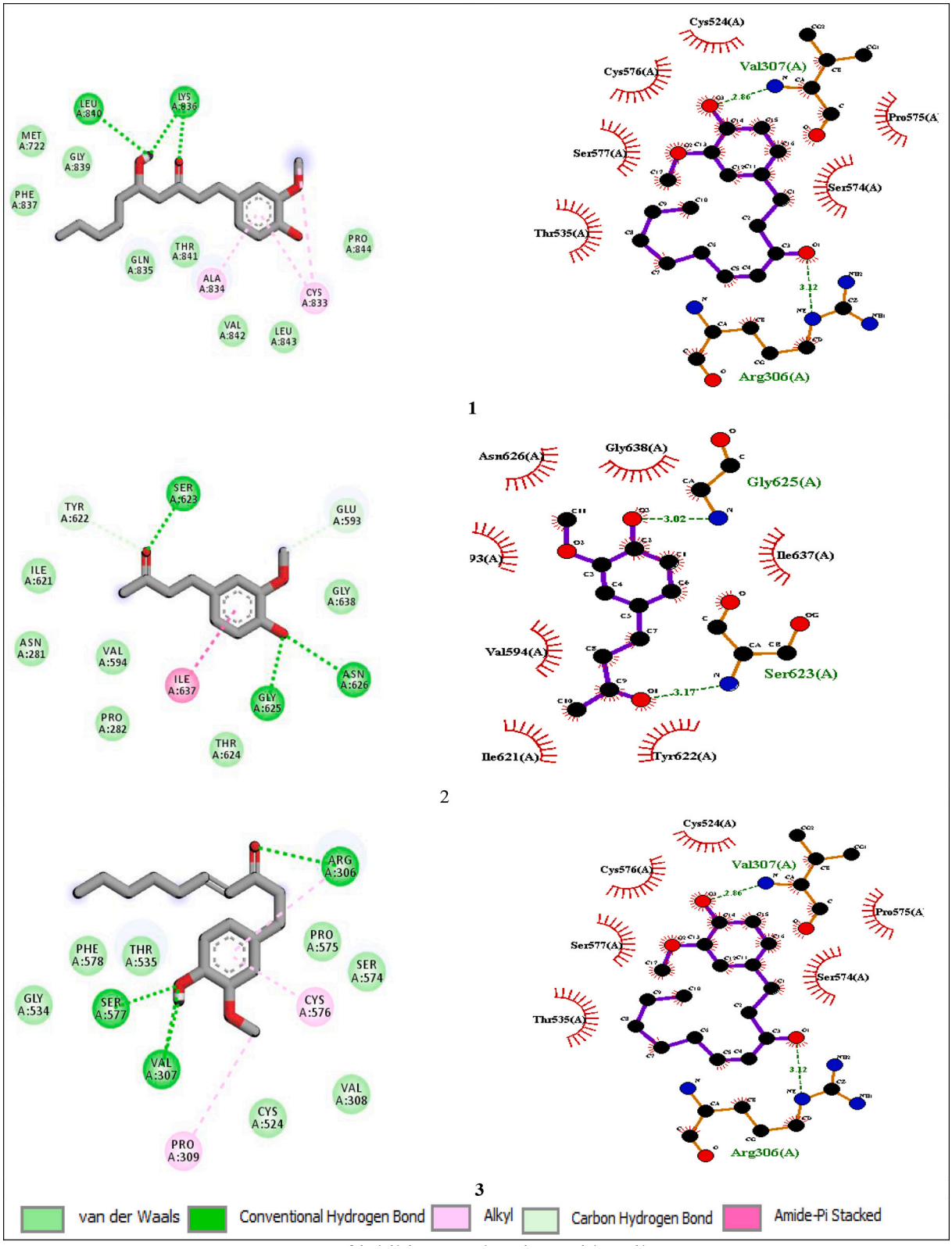

Fig. 9. 2D structures of inhibitors and amino acids spikes.

4. Conclusions

Inhibition of SARS-CoV-2 virus by active compounds derived from ginger 1, 2, and 3 was studied theoretically. The interaction of the proposed inhibitors with the virus's spikes was studied computationally. It was noticed that the inhibitors used the OH and C═O groups in the interaction with the protein of the virus spikes. By distinguishing electrophilic (+) and nucleophilic (−) atoms and utilizing Dual Descriptor used to predict the density of electron on the proposed inhibitors atoms. Obtained results in Mulliken charges were in good agreement with the FUKUI function. The strong affinity of the spike proteins to the ginger active compounds was reflected in the binding energy which was in the following order: $2 > 3 > 1$. According to the calculations, the studied compounds 1, 2, and 3 interacted with the spikes through hydrogen bonding, alkyl, and pi-alkyl.

Funding

Not applicable.

CRediT authorship contribution statement

Mustafa M. Kadhim: Data curation, Formal analysis, Software. **Anees A. Khadom:** Supervision, Visualization, Writing – review & editing. **Jawad Kadhim Abaies:** Conceptualization, Methodology. **Wesam R. Kadhum:** Writing – original draft. **Safa K. Hachim:** Software.

Declaration of competing interest

Authors hereby declare that they have no financial or personal interest regarding the submitted work.

Acknowledgments

The authors appreciate their employers (universities) for using the facilities.

References

Abdul, E., Fanfoon, D.Y., Al-uqaily, R.A.H., et al., 2021. Materials today: proceedings 1-Isoquinolinyl phenyl ketone as a corrosion inhibitor: a theoretical study. Mater Today Proc. 42, 2241–2246. https://doi.org/10.1016/j.matpr.2020.12.310.

Abolaji, A., Ojo, M., Afolabi, T.T., Arowoogun, M.D., Nwawolor, D., Farombi, E.O., 2017. Protective properties of 6-gingerol-rich fraction from Zingiber o_cinale (ginger) on chlorpyrifos-induced oxidative damage and inflammation in the brain, ovary, and uterus of rats. Chem. Biol. Interact. 270, 15–23.

B. AD, 1993. No TitleDensity-functional thermochemistry. III. The role of exact exchange. J. Chem. Phys. 98, 5648–5652.

Brendler, T., Al-Harrasi, A., Bauer, R., Gafner, S., Hardy, M.L., Heinrich, M., Williamson, E.M., 2021. Botanical drugs and supplements affecting the immune response in the time of COVID-19: implications for research and clinical practice. Phytother. Res. 35 (6), 3013–3031.

Dugasani, S., Pichika, M.R., Nadarajah, V.D., Balijepalli, M.K., Tandra, S., Korlakunta, J.N., 2010. Comparative antioxidant and anti-inflammatory effects of [6]-gingerol, [8]-gingerol, [10]-gingerol and [6]-shogaol. J. Ethnopharmacol. 127, 515–520.

Eva, A., Rana, A.A., Majid, H.A., Ivan, H.R., Mustafa, M.K., 2019. Electrochemical, morphological and theoretical studies of an oxadiazole derivative as an anti-corrosive agent for kerosene reservoirs in Iraqi refineries. Chem. Pap. 4, 9883–9892.

Frisch, Æ., Plata, R.E., Singleton, D.A., 2009. Gaussian 09W reference. J. Am. Chem. Soc. 137, 3811–3826. https://doi.org/10.1021/ja5111392.

Ghasemzadeh, A., Jaafar, H.Z., Rahmat, A., 2015. Optimization protocol for the extraction of 6-gingerol and 6-shogaol from Zingiber officinale var. rubrum theilade and improving antioxidant and anticancer activity using response surface methodology. BMC Complement. Altern. Med. 15, 258.

Ghasemzadeh, A., Jaafar, Hawa Z.E., Baghdadi, Ali, Tayebi-Meigooni, Amin, 2018. Formation of 6-, 8- and 10-Shogaol in ginger through application of different drying methods: altered antioxidant and antimicrobial activity. Molecules 23, 1646.

Hussein, E., Shaheed, I.M., Hatam, R.S., Kadhim, M.M., Al-kadhum, D.T., 2020. Adsorption, thermodynamic and DFT studies of removal RS dye on the Iraq clay from aqueous. Solutions 11, 495–502. https://doi.org/10.5530/srp.2020.3.63.

Iwasaki, Y., Morita, A., Iwasawa, T., Kobata, K., Sekiwa, Y., Morimitsu, Y., Kubota, K., Watanabe, T., 2006. A non-pungent component of steamed ginger-[10]-shogaol increases adrenaline secretion via the activation of TRPV1. Nutr. Neurosci. 9, 169–178.

Ji, K., Fang, L., Zhao, H., Li, Q., Shi, Y., Xu, C., Wang, Y., Du, L., Wang, J., Liu, Q., 2017. Ginger oleoresin alleviated gamma-ray irradiation-induced reactive oxygen species via the Nrf2 protective response in human mesenchymal stem cells. Oxidative Med. Cell. Longev. 2017, 1480294.

Kadhim, M., Kubba, R., 2020a. Theoretical investigation on reaction pathway, biological activity, toxicity and NLO properties of diclofenac drug and its ionic carriers. Iraqi J Kadhim and Kubba of Sci 61 (5), 936–951.

Kadhim, M., Kubba, R., 2020b. Theoretical investigation on reaction pathway, biological activity, toxicity and NLO properties of diclofenac drug and its ionic carriers. Iraqi J. Sci. 936–951. https://doi.org/10.24996/ijs.2020.61.5.1.

Kadhim, M., Salman, A., Zarzoor, A., Kadhum, W., 2021. Inhibition of SARS-CoV-2 reproduction using Boswellia carterii: a theoretical study. J. Mol. Liq. 337, 116440.

Khudhair, N., Kadhim, Mustafa M., Khadom, Anees A., 2021. Effect of trimethoprim drug dose on corrosion behavior of stainless steel in simulated human body environment: experimental and theoretical investigations. Bio- and Tribo-Corrosion 7 (124), 1–15.

Kumar, N., Murthy, P.S., Manjunatha, J.R., Bettadaiah, B.K., 2014a. Synthesis and quorum sensing inhibitory activity of key phenolic compounds of ginger and their derivatives. Food Chem. 159, 451–457.

Kumar, L., Chhibber, S., Harjai, K., 2014b. Hepatoprotective effect of zingerone (4-(4-hydroxy-3-methoxyphenyl) butane-2-one) in lipopolysaccharide-induced liver injury mouse model through downregulation of inflammatory mediators. Intern. J. Pharma. Phytochem. Res. 6 (2), 308–314.

Lee, C., Yang, W., Parr, R.G., 1988. Development of the Colle-Salvetti correlation-energy formula into a functional of the electron density. Phys. Rev. B 37, 785–789.

Li, H., Yu, C., Chen, R., Li, J., Li, J., 2012. Novel ionic liquid-type Gemini surfactants: synthesis, surface property and antimicrobial activity. Colloids Surf. A Physicochem. Eng. Asp. 395, 116–124.

Li, H., Leung, K.S., Ballester, P.J., Wong, M.H., 2014a. Istar: a web platform for large-scale protein-ligand docking. PLoS One 9, 85678. https://doi.org/10.1371/journal.pone.0085678.

Li, H., Leung, K.S., Ballester, P.J., Wong, M.H., 2014b. Istar: a web platform for large-scale protein-ligand docking. PLoS One 9, 85678. https://doi.org/10.1371/journal.pone.0085678.

Moon, Y., Lee, H., Lee, S., 2018. Inhibitory effects of three monoterpenes from ginger essential oil on growth and aflatoxin production of aspergillus flavus and their gene regulation in aflatoxin biosynthesis. Appl. Biol. Chem. 61, 243–250.

Mustafa, M., Abbas, W., Ameerah, M., Wesam, R.K., 2021. Inhibition of SARS-CoV-2 reproduction using Boswellia carterii: a theoretical study. J. Mol. Liq. 337, 116.

Okamoto, M., Hiroyuki Irii, Yu, Tahara, Hiroyuki Ishii, Hirao, Akiko, Udagawa, Haruhide, Hiramoto, Masaki, Yasuda, Kazuki, Takanishi, Atsuo, Shibata, Shigenobu, Shimizu, Isao, 2011. Synthesis of a new [6]-Gingerol analogue and its protective effect concerning the development of metabolic syndrome in mice fed a high-fat diet. J. Med. Chem. 54, 6295–6304.

Ownsend, E., Siviski, M.E., Zhang, Y., Xu, C., Hoonjan, B., Emala, C.W., 2013. Effects of ginger and its constituents on airway smooth muscle relaxation and calcium regulation. Am. J. Resp. Cell Mol. 48, 157–163.

Radhi, A., Du, Ennas A.B., Khazaal, Fatma A., Abbas, Zaid M., Aljelawi, Oday H., Hamadan, Salam D., Almashhadani, Haider A., Kadhim, Mustafa M., 2020. HOMO-LUMO energies and geometrical structures effect on corrosion inhibition for organic compounds predict by DFT and PM3 methods. NeuroQuantology 18, 37–45.

Sayin, K., Kariper, S.E., Taştan, M., Sayin, T.A., Karakaş, D., 2019. Investigations of structural, spectral, electronic, and biological properties of N-heterocyclic carbene ag(I) and Pd(II) complexes. J. Mol. Struct. 1176, 478–487. https://doi.org/10.1016/j.molstruc.2018.08.103.

Suk, S., Kwon, G.T., Lee, E., Jang, W.J., Yang, H., Kim, J.H., Thimmegowda, N.R., Chung, M., Kwon, J.Y., Yang, S., et al., 2017. Gingerenone a, a polyphenol present in ginger, suppresses obesity and adipose tissue inflammation in high-fat diet-fed mice. Mol. Nutr. Food Res. 61, 1700139.

Yaqo, E., Annee, R., Abdulmajeed, M., Tomi, I., Kadhim, M., 2019. Aminotriazole derivative as anti-corrosion material for Iraqi kerosene tanks: electrochemical, computational, and the surface study. Chemistry Select 4 (34), 9883–9892.

Yousef, T., Al-nassiry, A.I.A., 2020. Antimicrobial, Computational, and Molecular Docking Studies of Zn (Ii) and Pd (Ii) Complexes Derived From Piperidine Dithiocarbamate, pp. 1–15. https://doi.org/10.1002/aoc.6108.

Yu, J., Geng, Y.L., Wang, D.J., Zhao, H.W., Guo, L., Wang, X., 2018. Terpenes from the gum resin of Boswellia carterii and their NO inhibitory activities. Phytochem. Lett. 28, 59–63. https://doi.org/10.1016/j.phytol.2018.09.010.

Zhang, G., Nitteranon, V., Chan, L.Y., Parkin, K.L., 2013. Glutathione conjugation attenuates biological activities of 6-dehydroshogaol from ginger. Food Chem. 140 (140), 1–8.

Zhang, M., Viennois, E., Prasad, M., Zhang, Y., Wang, L., Zhang, Z., Han, M.K., Xiao, B., Xu, C., Srinivasan, S., et al., 2016. Edible ginger-derived nanoparticles: a novel therapeutic approach for the prevention and treatment of inflammatory bowel disease and colitis-associated cancer. Biomaterials 101, 321–340.

Zimmermann-klemd, A., Reinhardt, J.K., Nilsu, T., Morath, A., Falanga, C.M., Schamel, W.W., Huber, R., Hamburger, M., 2020. Fitoterapia Boswellia carteri extract and 3- O -acetyl-alpha-boswellic acid suppress T cell function. Fitoterapia 146, 104694. https://doi.org/10.1016/j.fitote.2020.104694.